

Supporting Information for

Multifunctional cell-culture-platform for aligned cell sheet monitoring, transfer printing, and therapy

Seok Joo Kim^{†,‡,#}, Hye Rim Cho^{†,§,#}, Kyoung Won Cho^{†,‡,#}, Shutao Qiao[⊥], Jung Soo Rhim[⊥], Min Soh^{†,‡}, Taeho Kim^{†,‡}, Moon Kee Choi^{†,‡}, Changsoon Choi^{†,‡}, Inhyuk Park^{†,‡}, Nathaniel S. Hwang[‡], Taeghwan Hyeon^{†,‡}, Seung Hong Choi^{†,§,*}, Nanshu Lu^{⊥,*}, Dae-Hyeong Kim^{†,‡,*}

[†]*Center for Nanoparticle Research, Institute for Basic Science (IBS), Seoul 151-742, Republic of Korea*

[‡]*School of Chemical and Biological Engineering, Institute of Chemical Processes, Seoul National University, Seoul 151-742, Republic of Korea*

[§]*Department of Radiology, Seoul National University College of Medicine, Seoul 110-744, Republic of Korea*

[⊥]*Center for Mechanics of Solids, Structures, and Materials, Department of Aerospace Engineering and Engineering Mechanics, Texas Materials Institute, University of Texas at Austin, 210 E 24th Street, Austin, Texas 78712, USA*

[⊥]*School of Mechanical and Aerospace Engineering, Seoul National University, Seoul 151-742, Republic of Korea*

[#]*S. J. Kim, H. R. Cho and K. W. Cho contributed equally to this work.*

^{*}*Address correspondence to dkim98@snu.ac.kr, nanshulu@utexas.edu, verocay@snuh.org*

This Supporting information contains:

Text, Table, and Figures

1. Text

1.1. FEM and analytical modeling of energy release rate vs. crack length

Abaqus 6.10 is used to perform finite element modeling (FEM) to study the relation between energy release rate and crack length when peeling a soft PDMS film from a glass substrate as shown in Figure S9a in the Supporting Information. We simplify the problem to be 2-dimensional plane strain and the boundary conditions we applied are: i) the bottom of the glass slide is fixed; ii) the left edge of the PDMS film is loaded by either fix force F or fix deflection Δ , for different crack size a . The PDMS film is modeled as Neo-Hookean material while the glass slide is treated as elastic material and their mechanical properties as well as geometries are shown in Table S1 in Supporting Information. The crack is defined as a seam with length a on the PDMS/Glass interface (the red solid line in Figure S9a in the Supporting Information) and near the crack front an integral path (the yellow circular path in the zoomed in picture in Figure S9a in the Supporting Information) is assigned for the J -integral to obtain the energy release rate at the crack tip. Path independence of the J -integral has been checked and ensured. The overall structure is meshed by quadratic quadrangle CPE8RH element except near the crack tip (quadratic triangular CPE8RH element) and the results are plotted in Figure S9b in the Supporting Information by solid circular dots for both force control under $F_1 = 0.01$ N/m (blue) and $F_2 = 0.02$ N/m (red) and displacement control under $\Delta_1 = 300$ μm (blue) and $\Delta_2 = 600$ μm (red).

Since the glass is much stiffer compared to the PDMS, analytical approximations can be made by neglecting the deformation of the glass slide and treating the debonded part

of the PDMS film as a cantilever beam (of length a) undergoing small deflection due to the applied loadings (F or Δ). Then the total strain energy U can be expressed as

$$U = \frac{F^2 a^3}{6\bar{E}I} = \frac{3\Delta^2 \bar{E}I}{2a^3} \quad (\text{S1})$$

where $\bar{E}I$ is the bending rigidity of the PDMS film and

$$\frac{F}{\Delta} = \frac{3\bar{E}I}{a^3} \quad (\text{S2})$$

Thus, the energy release rate is

$$G = \left(\frac{\partial U}{b \partial a} \right)_F = \frac{\partial}{b \partial a} \left(\frac{F^2 a^3}{6\bar{E}I} \right) = \frac{F^2 a^2}{2\bar{E}I} \quad (\text{S3})$$

for force control and

$$G = \left(-\frac{\partial U}{b \partial a} \right)_\Delta = -\frac{\partial}{b \partial a} \left(\frac{3\Delta^2 \bar{E}I}{2a^3} \right) = \frac{9\Delta^2 \bar{E}I}{2a^4} \quad (\text{S4})$$

for displacement control where b is the out of plane thickness for the bilayer structure and is set to be unit length for the plane strain problem. These analytical approximations are plotted as solid curves in Figure S9b in the Supporting Information which compares favorably with the FEM results. It is noticed that under force control, the energy release rate increases monotonically with both force and crack length, which serves as the foundation of our explanations for cell sheet transfer given in Figure 5.

1.2. Effect of PDMS margin size

PDMS margin size, which is defined as the distance between the edge of graphene and the edge of PDMS, is experimentally found to be a significant control parameter on the yield of cell sheet transfer printing, as shown in the right frame of Figure 5f. It is observed that the transfer yield is lower than 40% when there is no margin, *i.e.* when the whole surface of the PDMS is covered by graphene and cell sheet. In our fracture mechanics model, we

assume that only cell sheets are adhered to polystyrene, hence bare PDMS to polystyrene contact zone is considered as the initial interface crack and therefore the margin size is the initial crack size. The stress state at the edge of the cell sheet looks very different when there is or is not margin, as shown in Figure S10 in the Supporting Information. FEM is applied via Abaqus 6.10 and results are plotted in Figure S10b in the Supporting Information as solid circular dots for different margin size: 0 μm (blue), 500 μm (red) and 1000 μm (green). As we can see from Figure S10b in the Supporting Information, larger margin size does give us higher normal stretching stresses near the edge of cell sheet when peeling the PDMS off polystyrene, which leads to a larger damaged cell zone, and hence larger effective crack size. Figure S10c in the Supporting Information offers the contour plots of the stress field for different margin sizes. Higher stress is found when the margin size is larger.

1.3. Effect of cell sheet moisture

Water can migrate through cell sheet due to capillary effect and then wet the graphene/cell interface such that the adhesion of graphene/cell can be reduced,¹ *e.g.* from $\Gamma'_{C/Graph}$ to $\Gamma_{C/Graph}$ in Figure S11b in the Supporting Information. The critical forces for PDMS/graphene and cell/graphene interfacial cracks to propagate are represented by F_3 and F_2 , respectively. After moisture added in between of graphene and cell sheet, the previously stronger adhesion $\Gamma'_{C/Graph}$ ($\Gamma'_{C/Graph} > \Gamma_{PDMS/Graph}$) now becomes the weaker one ($\Gamma_{C/Graph} < \Gamma_{PDMS/Graph}$) such that the critical force for cell/graphene crack propagation is smaller than that of PDMS/graphene ($F_2 < F_1$). Thus, when peel PDMS off

the wet sample, graphene remains attached on PDMS, as illustrated by Figure S11c in the Supporting Information.

1.4. Effect of cell sheet continuity

For discontinuous cell sheet, though stretching effect can still be induced in preparation step, due to the existence of the gaps in between of neighboring cell islands, the stretching effect of the cell can be relaxed and such that the shear-induced crack size is not as significant as that of continuous cell sheet (see Figure S12a in the Supporting Information).

With $\Gamma_{C/Graph}$ and $\Gamma_{C/Glass}$ unchanged, a larger force is needed to initiate crack propagation for cell/graphene interface (F_2) than that for cell/glass interface (F_1) as shown in Figure S12b in the Supporting Information, which means, when quasi-statically increasing the applied force F , the crack of the cell/glass interface begins to propagate first, *i.e.* sample will stay with graphene and be peeled off from glass.

Reference

1. Kasemo, B. Biological surface science. *Surf. Sci.* **2002**, *500*, 656-677.

2. Table

Table S1. Properties of the PDMS film and the glass slide

	Young's Modulus	Poisson's Ratio	Thickness (μm)	Material Model
PDMS	36 KPa	0.49	500	Neo-Hookean
Glass	70 GPa	0.3	1000	Linear Elastic

3. Figures

See next pages.

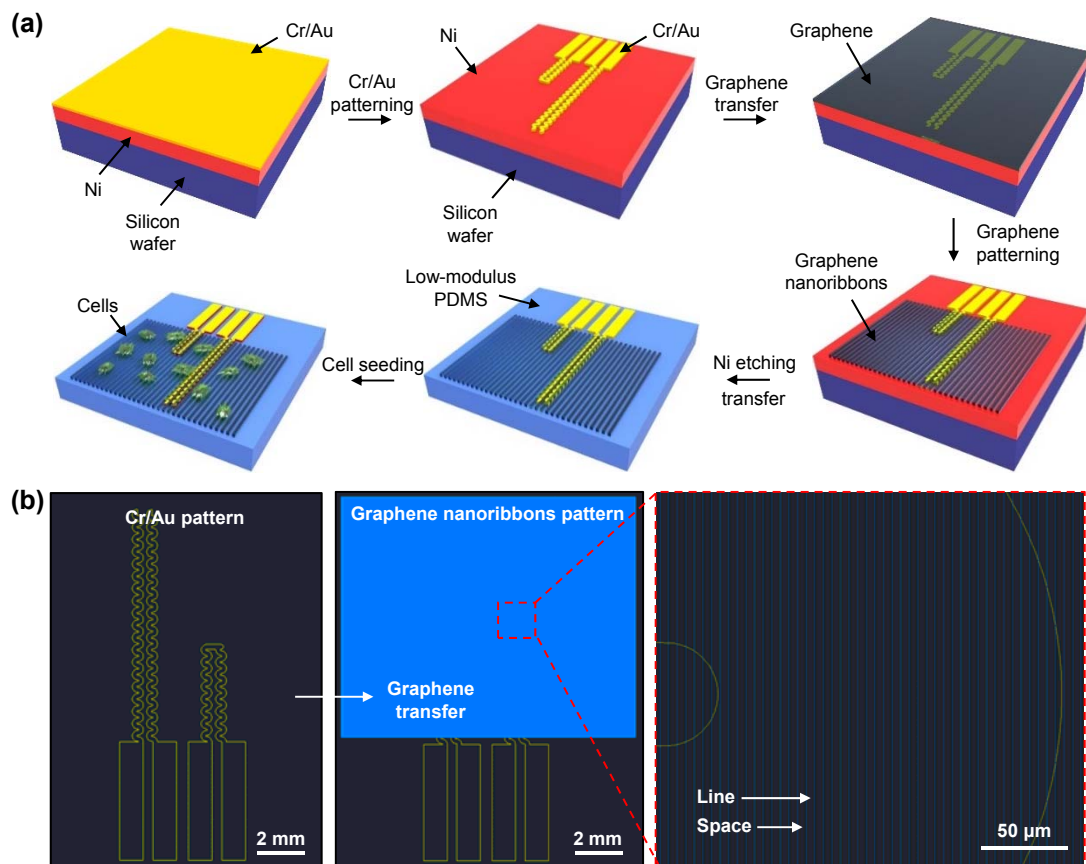


Figure S1. Detailed fabrication process of the stretchable instrumented cell-culture-platform. (a) A schematic overview of the fabrication process. (b) AutoCAD designs of impedance and temperature sensors, along with the patterned graphene nanoribbons.

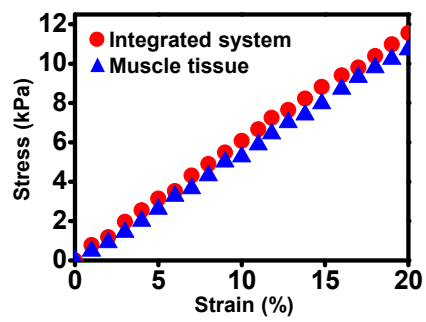


Figure S2. Stress-strain curve for system modulus of integrated system and muscle tissue.

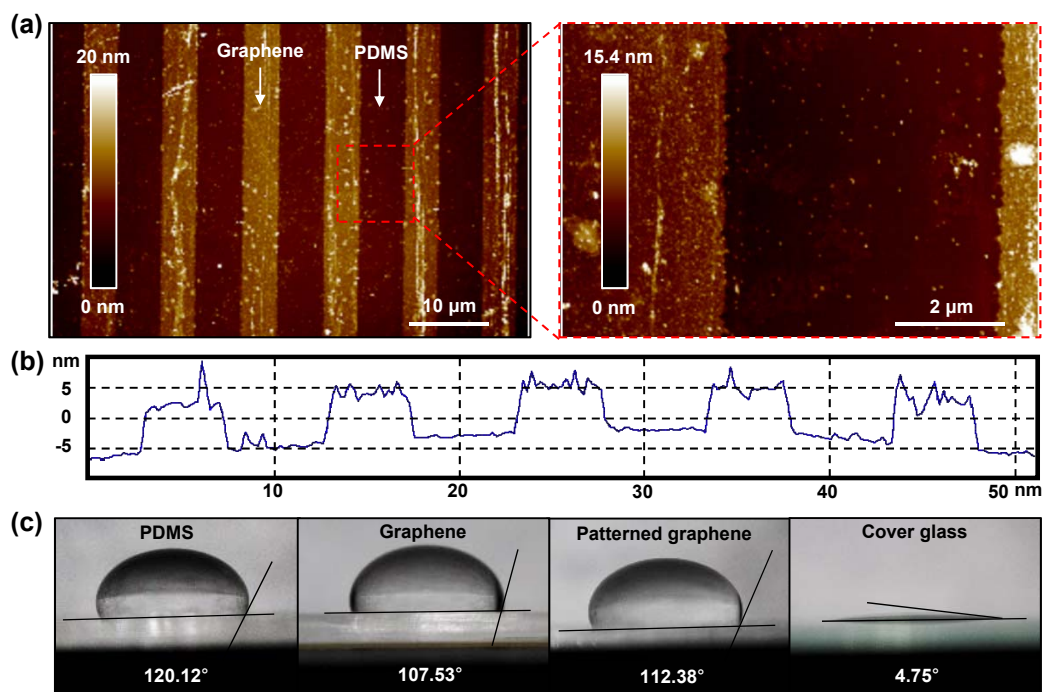


Figure S3. Characterization of patterned graphene nanoribbons. (a) AFM topological image of the patterned graphene on PDMS. Spring constants of cantilevers (TESP, Bruker probes) is 42 N/m and all AFM data are measured with a tapping mode. Data are visualized by the NanoScope Analysis software (Bruker). (b) AFM topological graph of patterned graphene on PDMS. (c) Water contact angles of various substrates: PDMS, graphene, patterned graphene (widths of line and spacing; 5 μm), and cover glass.

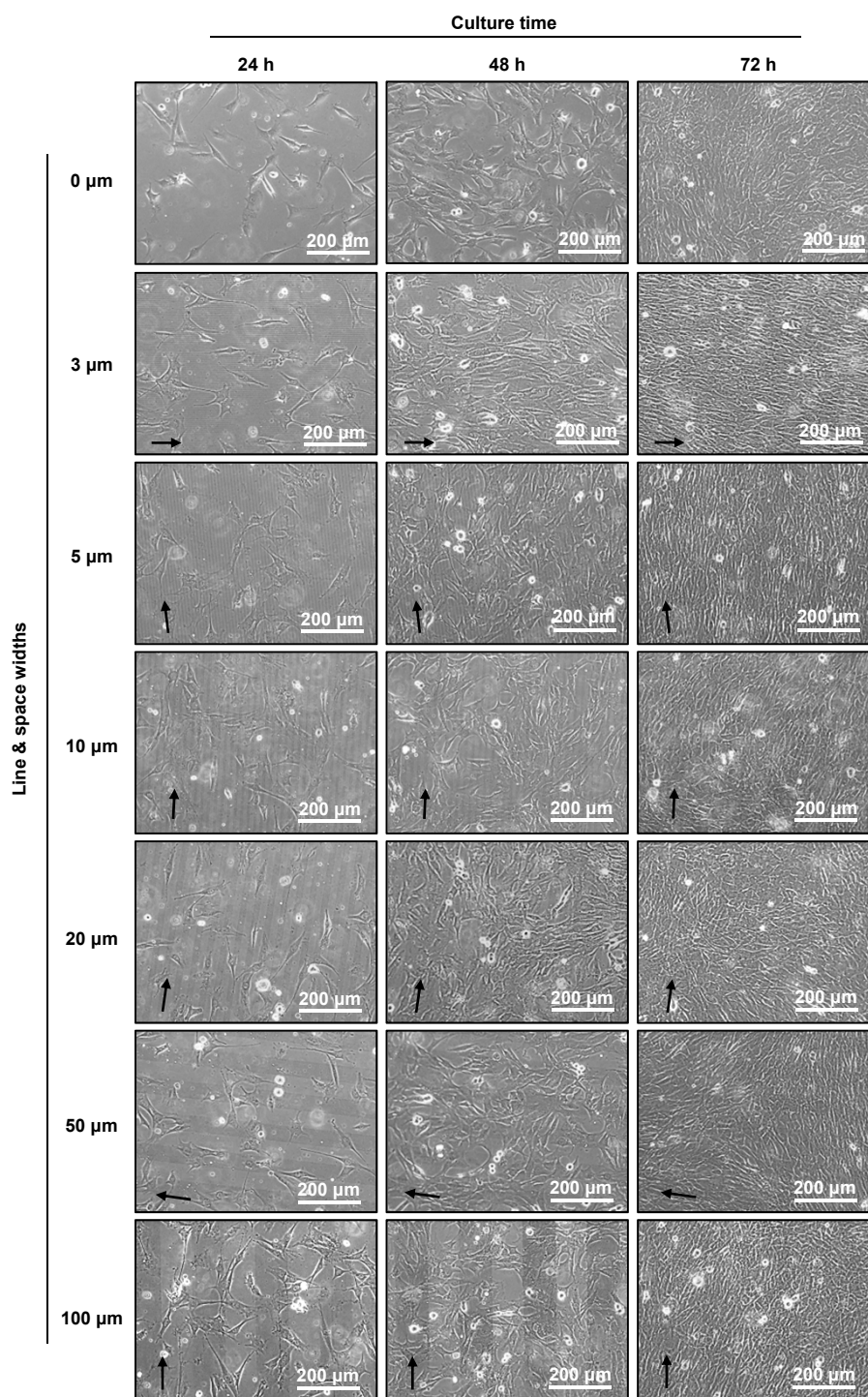


Figure S4. Phase-contrast microscope images of cell alignments in respect to pattern sizes and culture time. C2C12 myoblasts are cultured on the 7 different graphene patterns with different line and space widths (0, 3, 5, 10, 20, 50, and 100 μm) to find the best pattern width for cell alignments. Each sample is observed at three different time (24, 48, and 72 h after the culture) by the phase-contrast microscopy.

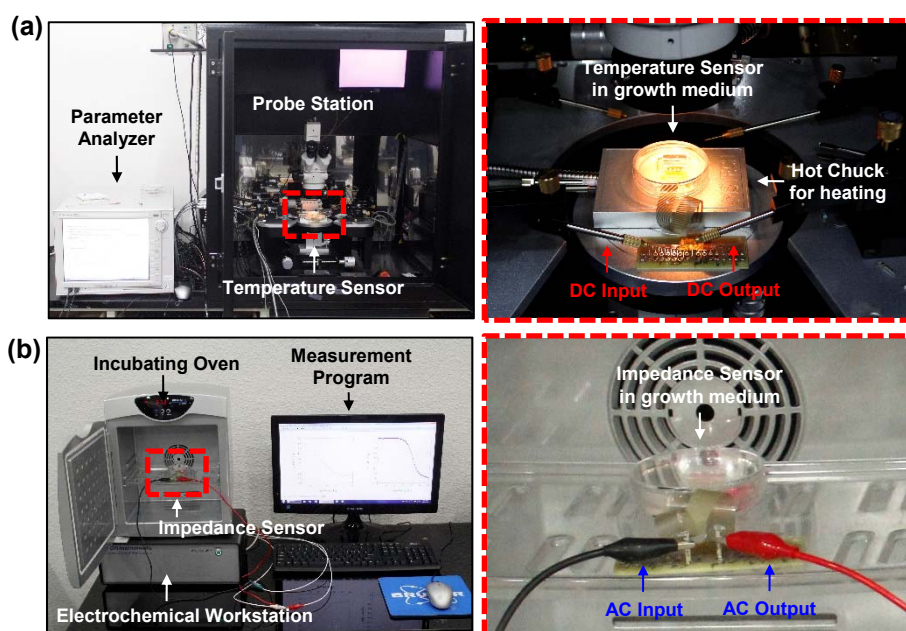


Figure S5. Images of experimental setups for the sensor characterization. (a) Characterization of the temperature sensor in the growth medium by the probe station and parameter analyzer. For heating, the sensor is placed on a hot chuck. (b) Characterization of the impedance sensor in the growth medium by the electrochemical workstation while maintaining its environment temperature as 37 °C in an incubating oven.

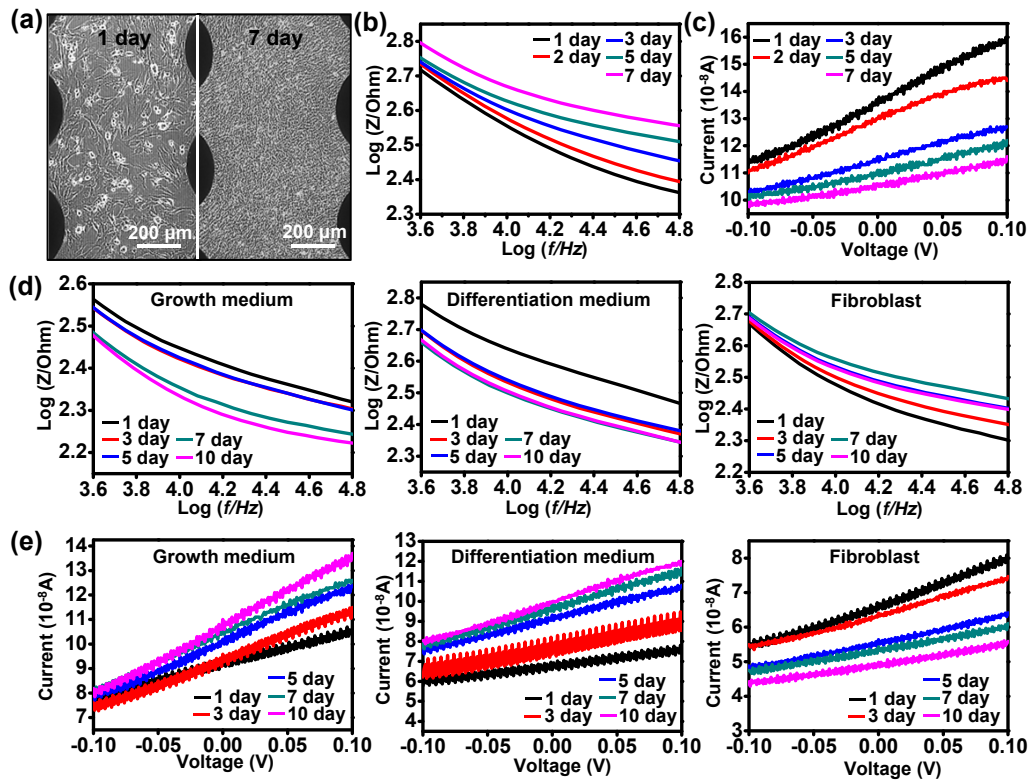


Figure S6. Impedance change during proliferation and differentiation of C2C12 myoblasts. (a) Phase contrast microscope images of C2C12 myoblasts proliferating on the instrumented cell-culture-platform after 1 and 7 days of culture. Time-dependent changes of (b) impedance and (c) I-V curve as the C2C12 myoblasts proliferate. (d) Time-dependent impedance change during the differentiation of C2C12 myoblasts cultured in the growth medium (left) and differentiation medium (middle). The right frame shows the impedance change of fibroblast in the growth medium (control). (e) Time-dependent I-V curve changes during the differentiation of C2C12 myoblasts cultured in the growth medium (left), and differentiation medium (middle). The right frame shows the I-V curve change of fibroblast in growth medium (control).

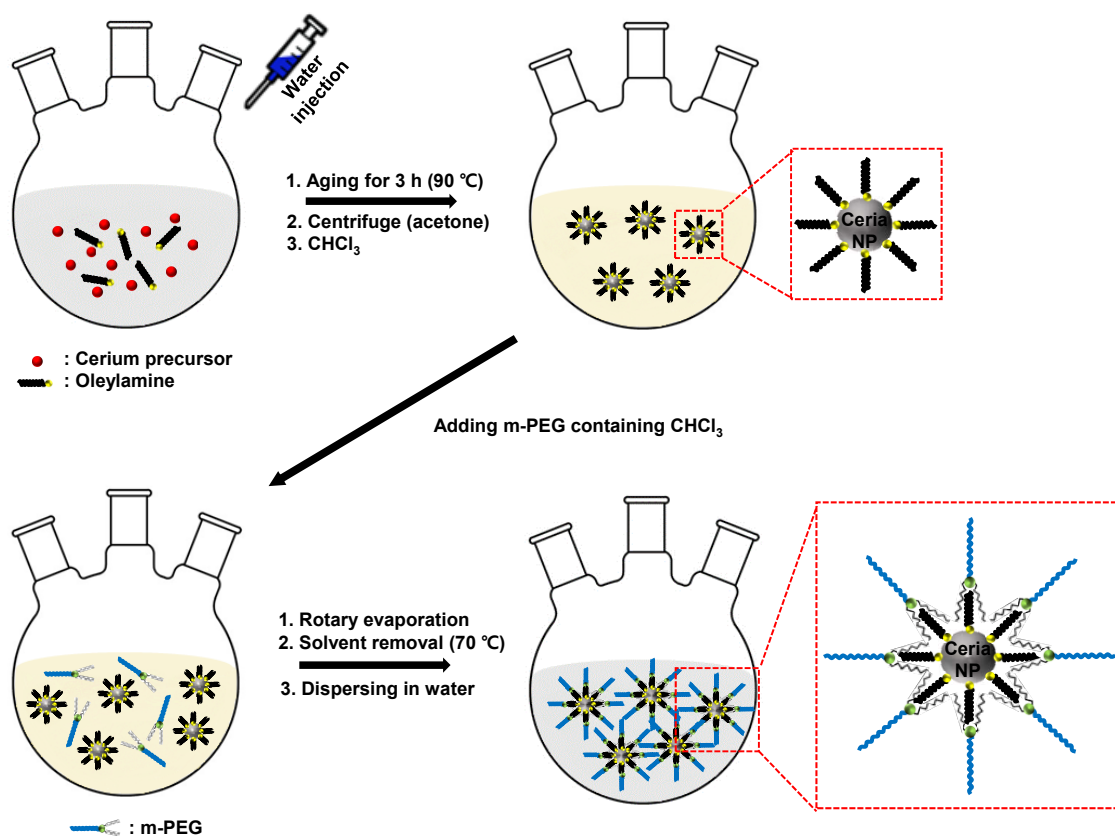


Figure S7. A schematic overview of the synthesis process of ceria nanoparticles.

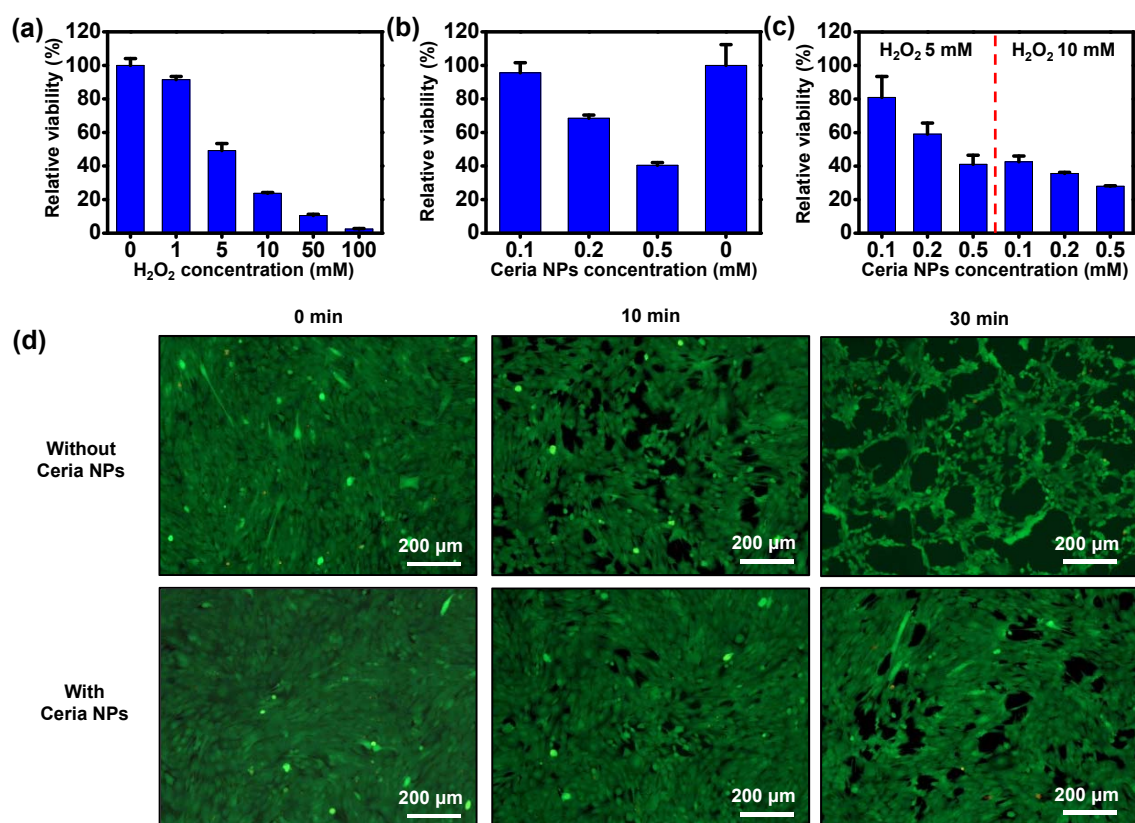


Figure S8. Effects of ceria nanoparticles on cellular viability. A plot of relative viability of cells depending on the concentration of (a) hydrogen peroxide (H_2O_2) and (b) ceria nanoparticles (Ceria NPs). (c) A graph of relative viability of cells versus concentrations of Ceria NPs with 5 mM and 10 mM of H_2O_2 treatments. All data are acquired after treating H_2O_2 and Ceria NPs for 30 min, then the samples are incubated in the MTT solution (Amresco) for 3 h. Data are quantified by using a microplate reader (SpectraMax M3, Molecular Devices). (d) Fluorescence images of H_2O_2 -exposed C2C12 cells with/without Ceria NPs at different time periods. H_2O_2 -exposed cells with/without Ceria NPs are stained with LIVE/DEAD Viability Kit and observed by a fluorescence microscopy.

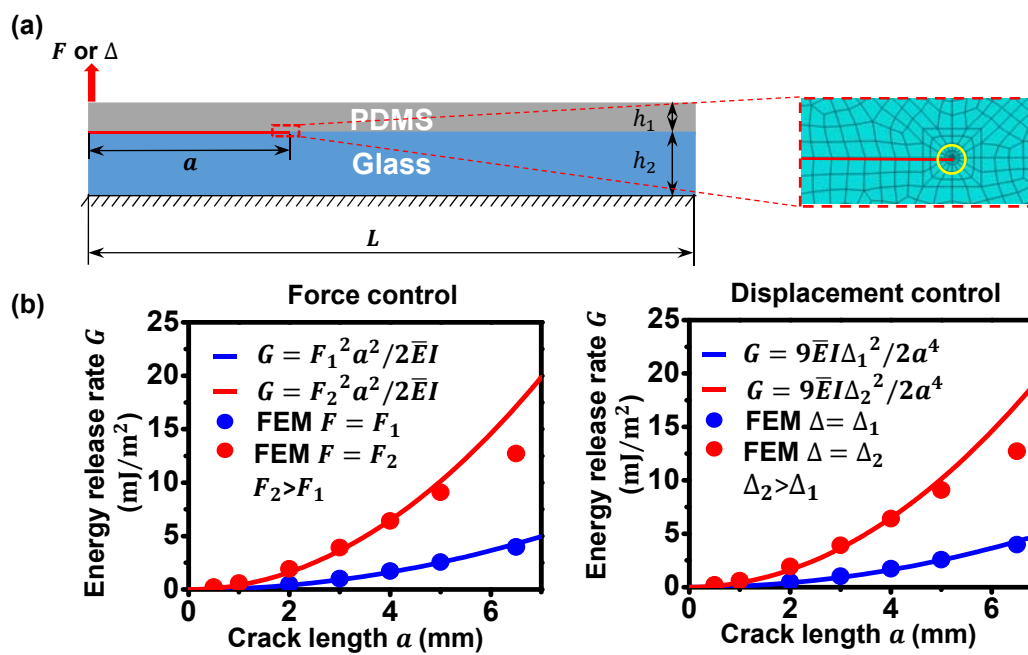


Figure S9. Theoretical analysis for crack propagation in cell sheet. (a) FEM simulation of PDMS/Glass interfacial crack under force control (F) or displacement control (Δ). (b) Comparison of $G \sim a$ relations between the FEM results (dots) and the analytical approximations (curves) for both the force control under $F_1 = 0.01$ N/m (blue) and $F_2 = 0.02$ N/m (red) and the displacement control under $\Delta_1 = 300$ μm (blue) and $\Delta_2 = 600$ μm (red).

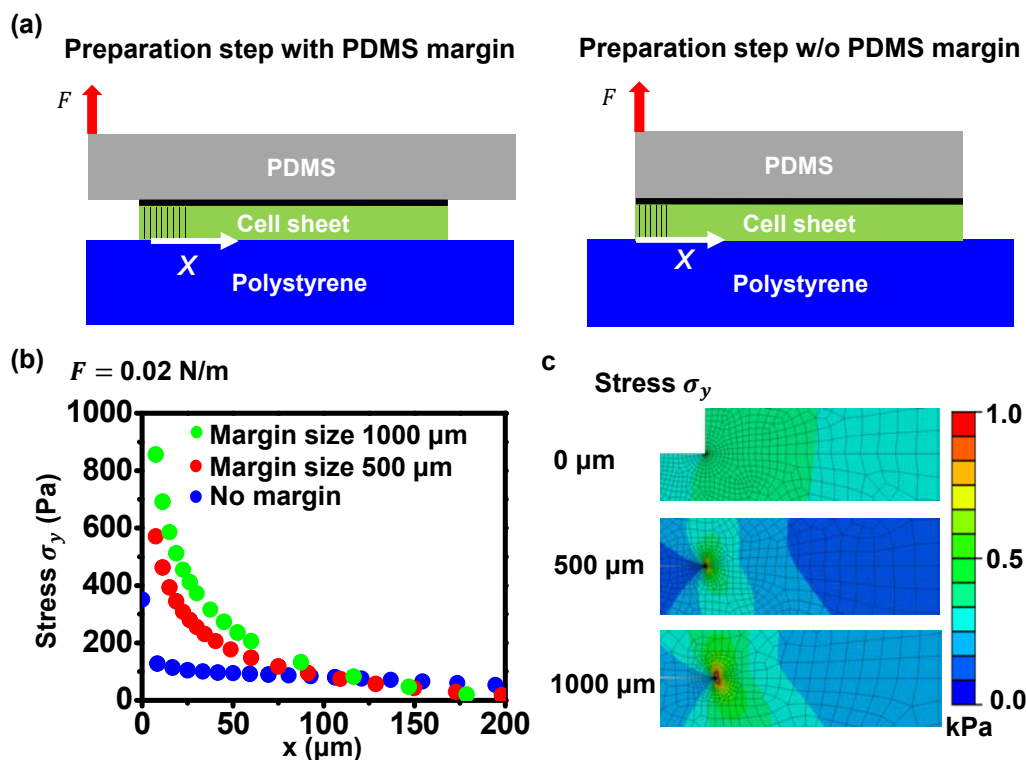


Figure S10. Theoretical analysis for the effect of PDMS margin on cell sheet transfer printing. (a) Schematic images for the preparation step with or without PDMS margin. (b) Comparison of the FEM results (solid circular dots) of the stress (σ_y) distributions along the cell/PS interface between different margin sizes: 0 μm (blue), 500 μm (red) and 1000 μm (green). Axis x is shown in (a) pointing along the interfacial direction and axis y is in the perpendicular direction of axis x . The force applied in the 2D FEM model is 0.02 N/m. (c) FEM contour plot of stress distribution (σ_y) near the cell sheet edge for different margin sizes: 0 μm , 500 μm and 1000 μm .

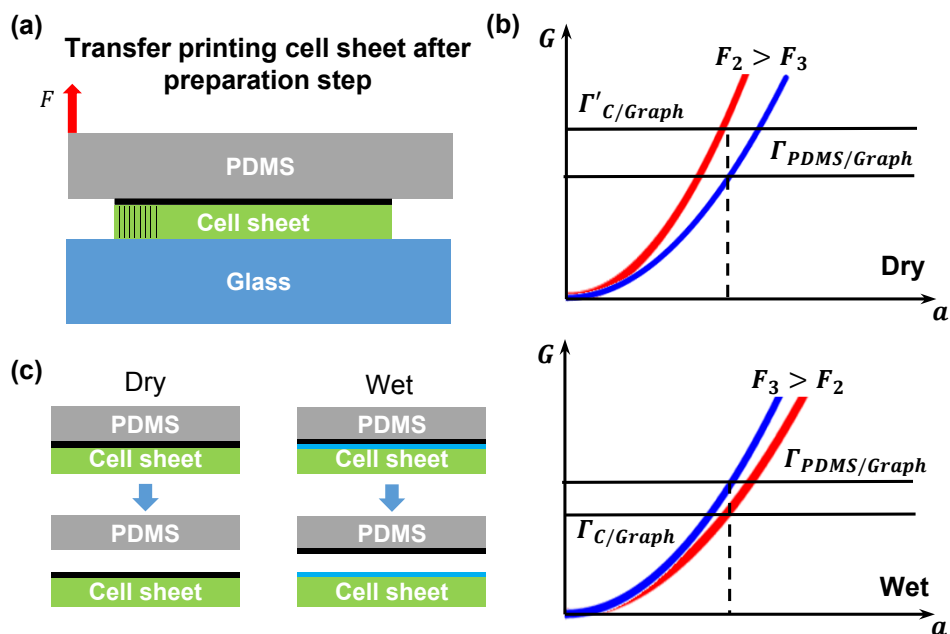


Figure S11. Theoretical analysis for the effect of moisture on cell sheet transfer printing. (a) Schematic image of transfer printing cell sheet after preparation step. (b) Moisture is considered to be a factor that reduces the adhesion of cell/graphene interface which lower the critical force needed for crack of cell/graphene interface to propagate. (c) After transferring, the graphene layer remains on the cell sheet for dry samples but stays with PDMS for wet samples.

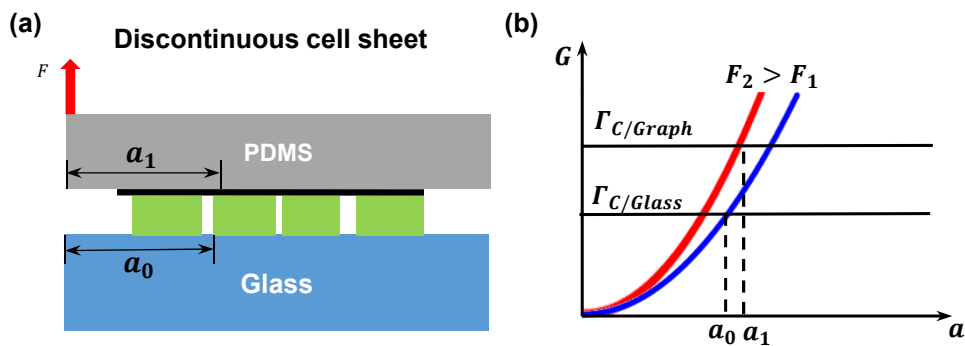


Figure S12. Theoretical analysis for the effect of cell sheet continuity on transfer printing. (a) Schematic image of a sample with discontinuous cell sheet on glass after preparation step. The sizes of cell/glass crack and effective cell/graphene interface crack are denoted by a_0 and a_1 , respectively. (b) Due to the relaxation of gaps between neighboring cell islands, the stretch induced increase of the crack length of cell/PDMS interface is not significant. Thus, though a_1 is greater than a_0 , the critical force for crack propagation of cell/graphene interface is larger than that of cell/glass interface ($F_2 > F_1$), i.e. crack propagation will firstly happen on cell/glass interface.

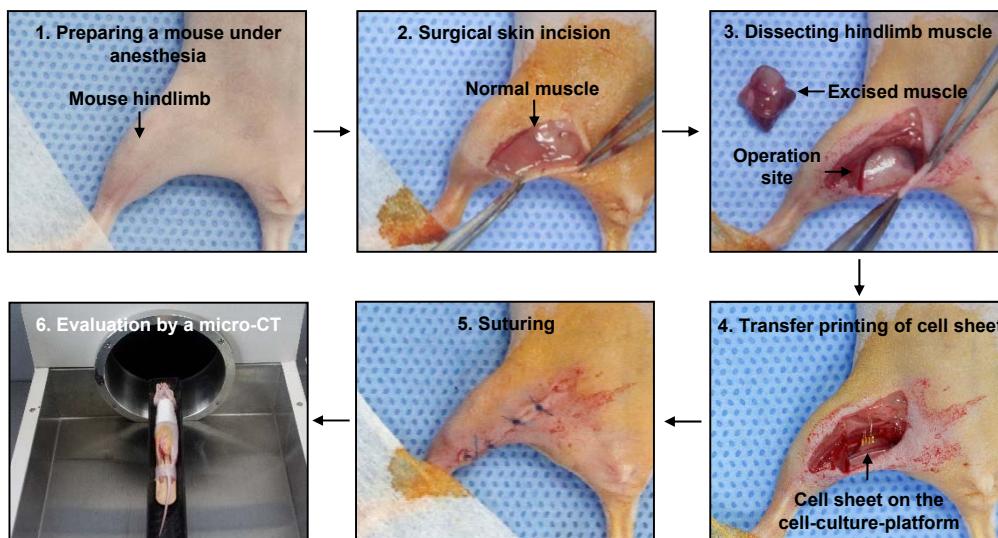


Figure S13. Images of surgery and cell sheet transfer-printing in the scarred muscle model of a mouse.

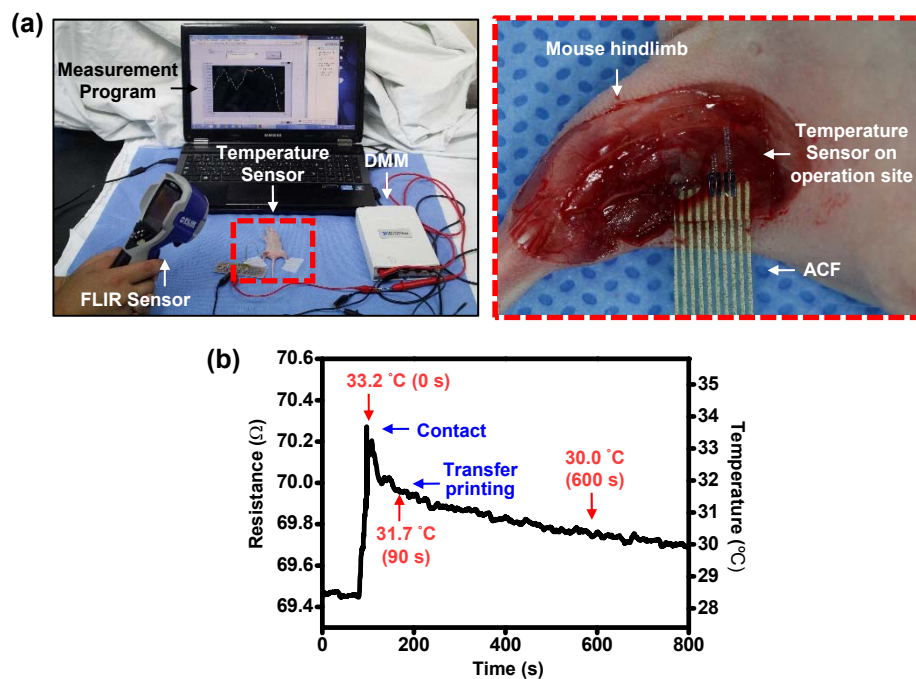


Figure S14. Measurement of temperature change with the instrumented cell-culture-platform during transfer-printing of the cell sheet *in vivo*. (a) Images of the temperature sensing experiment. After dissecting muscle, the ACF-connected instrumented cell-culture-platform is placed on the operation site. Then, the time-dependent resistance change of the temperature sensor is measured over 10 min with a Digital Multimeters (DMM, National Instrument) and the data is plotted in (b). The time-dependent temperature is also measured simultaneously by the commercial optical thermometer which is indicated by red arrows.

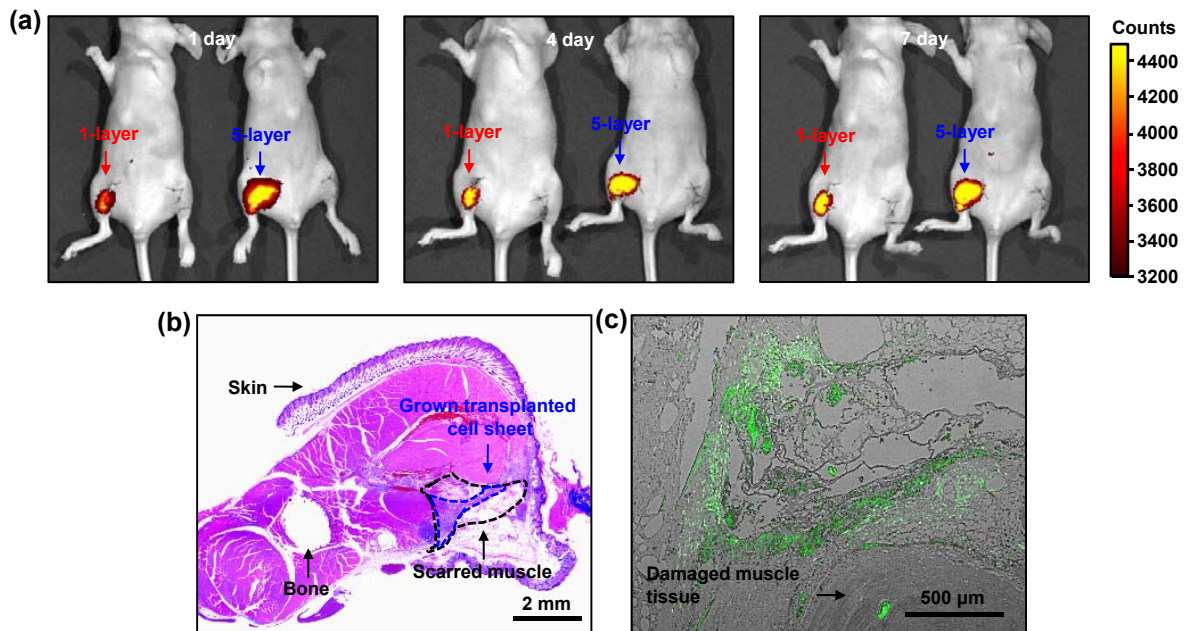


Figure S15. The fluorescence images and histological analysis of mice transplanted with cell sheet. (a) The fluorescence images show that both 1-layer and 5-layer of transplanted cell sheets maintain their structure and original location for over 7 days. (b) Image of H&E staining and (c) fluorescence image of the transplanted cell sheet expressing GFP for histological analysis of the monolayer cell sheet transplanted at the scarred region.

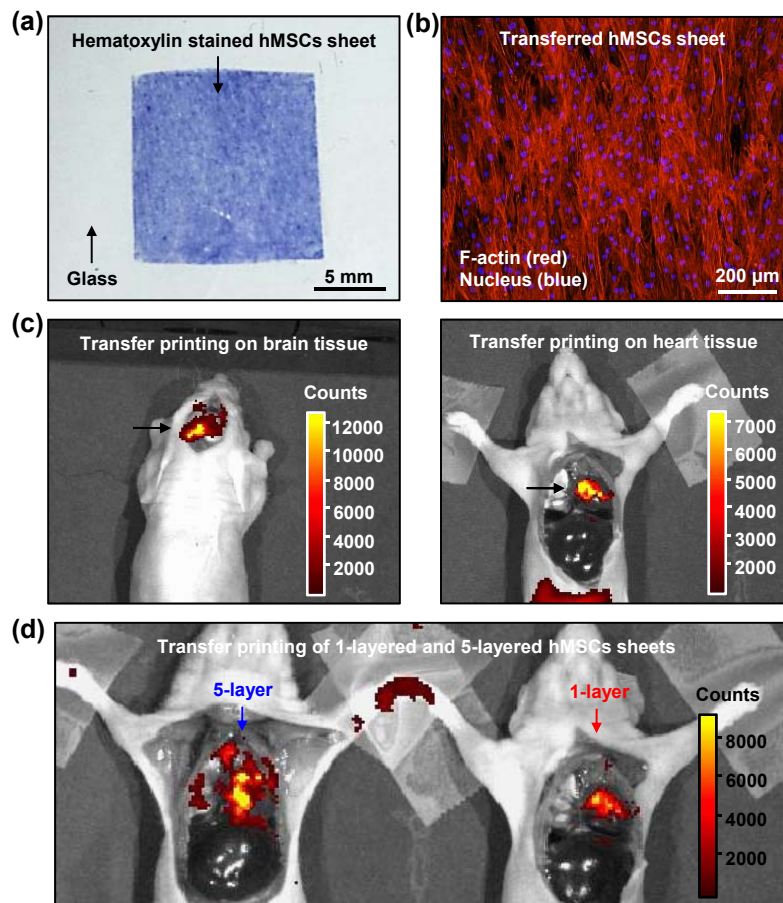


Figure S16. Transfer printing of hMSCs sheet. (a) Observation of hMSCs sheet after transfer printing onto the protein coated glass by staining the cells with hematoxylin. (b) The maintenance of cytoskeletal organization of hMSCs sheet after transfer printing on the glass. (c) The fluorescence images of the hMSCs sheet transfer-printed onto brain (left) and heart (right) tissues. For cell sheet transplantation, brain and heart of anesthetized mice are exposed by surgery. (d) The fluorescence image of the multiple transfer printings of hMSCs sheets (five sheets in total) onto the heart tissues. Left and right show experimental and control image, respectively.